Article

Microscopic Effect of Mixed Wetting Capillary Characteristics on Spontaneous Imbibition Oil Recovery in Tight Reservoirs

Yu Pu [1,2], Erlong Yang [1,*] and Di Wang [2,3]

[1] Key Laboratory of Ministry of Education for Enhancing Oil and Gas Recovery, Northeast Petroleum University, Daqing 163318, China; dongyoupuyu@nepu.edu.cn

[2] School of Architecture and Civil Engineering, Northeast Petroleum University, Daqing 163318, China; wangdinepu@stu.nepu.edu.cn

[3] Heilongjiang Provincial Key Laboratory of Thermal Utilization and Disaster Reduction of New Energy in Cold Regions, Northeast Petroleum University, Daqing 163318, China

* Correspondence: wangdidbsy@nepu.edu.cn

Abstract: The understanding of the mechanisms that govern water spontaneous imbibition in mixed wetting capillary channels plays a significant role in operating the oil extraction and energy replenishment for the tight oil reservoirs. In this work, the conservative form phase-field model together with the Navier–Stokes equation is employed to investigate the influence of the mixed wetting distribution and the wetting degree on the imbibition oil recovery effects and microscopic flow characteristics. Results indicate that there exist different oil detachment modes of spontaneous imbibition, and these modes are determined by the coupled effect of mixed wetting fraction and contact angle size. For the mixed wetting capillary with strong oil wetting, when f_w is low, spontaneous imbibition can only partially detach the oil. Low f_w slows down the fluid flow velocity and leads to the small imbibition oil recovery rate. After that, the influence of the surface contact angle size of the mixed wetting capillary is discussed. For the complete detachment mode, the capillary tube presents a form of water phase saturated filling, achieving the optimal imbibition oil recovery effect. For the mixed wetting capillary tube with the combination of weak water wetting and strong oil wetting (i.e., $\theta_w = 75°$ and $\theta_o = 165°$), local spontaneous imbibition turbulence can only detach very little oil at the inlet of the water wetting area, ultimately achieving a recovery efficiency of less than 10%. This work illuminates the spontaneous imbibition oil recovery mechanisms and flow potentiality for the different mixed wetting capillary channels.

Keywords: tight reservoirs; mixed wettability; pore scale; imbibition mechanism; oil detachment

1. Introduction

Tight oil has rich reserves and significant resource potential. It is considered a realistic alternative for oil replacement [1,2]. However, due to the strong heterogeneity and poor physical properties of tight oil reservoirs, current development methods mainly combine horizontal well volume fracturing with depletion development. Additionally, the rapid attenuation of formation energy results in a primary oil recovery factor that is generally below 10% of the original oil in place [3,4]. In tight oil reservoirs, the development of micro- and nano-scale pores is common. These pores exhibit strong capillary forces, making imbibition a dominant mechanism for oil extraction and energy replenishment in tight reservoirs [5,6].

Capillary pressure causes the wetting phase (i.e., water) to be imbibed into the tight porous medium. This process displaces the original oil in the porous media. Capillary pressure, which drives imbibition, is closely linked to the wettability of pore surfaces [7]. Siebold et al. [8] studied the spontaneous imbibition process of different fluids in a single capillary. They found that the wettability of pore walls is related to the fluid imbibition velocity. In water wetting reservoirs, a smaller contact angle leads to better oil recovery through imbibition. This results in a greater fluid imbibition migration distance [9]. The mechanism of imbibition oil recovery in these reservoirs involves water being drawn into small pores and then discharged from larger ones [10]. In contrast, imbibition oil recovery is not feasible in oil wetting reservoirs because it cannot overcome flow resistance [11]. To initiate oil detachment in the pores, chemical agents must be used to improve the pore surface wettability from oil wetting to water wetting [12]. Although the mechanisms of imbibition oil recovery for different wetting reservoirs have been clarified, current research mainly focuses on single-wetting reservoirs.

However, not all of the reservoirs are uniformly wetting. The mineral composition of tight oil reservoirs is complex and randomly distributed, leading to uneven wettability distribution on the rock pore surfaces. This is commonly manifested as a mixed wettability pattern, with partial water wetting and partial oil wetting [13,14]. The surfaces of some micro- and nano-pores containing rich asphalt exhibit strong oil wetting states, while pores composed of inorganic minerals exhibit typical water wetting states [15–17]. In addition, the oil phase containing the polar organic compounds with interfacial activity invades the water wetting water-saturated rock pores, which also makes the tight oil reservoirs show obvious dual wetting characteristics [18]. There are varying degrees of wetting effects between the fluid and the reservoir pore interfaces, which makes the micro distribution of oil and water, the mechanism of rock–water–oil interaction, and the energy transfer law of the oil stripping process more complex inside the reservoir [19]. This complex mixed wetting characteristic will also inevitably affect the oil detachment mode within the pore channels of porous media, leading to differences in the mechanisms of oil detachment, detachment efficiency, and the flow characteristics of oil under varying conditions. This finally leads to the complexity of the spontaneous imbibition process of tight porous media in space and time, directly affecting the evolution characteristics of the spontaneous imbibition in the pores [20]. CT research has shown that the flow mechanisms in the spontaneous imbibition for water wetting and mixed wetting porous media are different [21]. Only in the water wetting porous media can a clear spontaneous imbibition saturation front be formed, while in the mixed wetting porous media, only local imbibition filling occurs [22,23]. There is little literature on quantitatively characterizing the front distance and oil detachment in mixed wetting channels during the spontaneous imbibition process. Research has found that the water wetting pores in mixed porous media play a dominant role in the process of imbibition oil recovery. Moreover, the higher the proportion of water wetting pores, the better the spontaneous imbibition oil recovery effect is [24,25]. Although a strong correlation is observed between the oil imbibition efficiency and the mixed wetting degree (i.e., the mixed wetting fraction), the logic behind this parameter and its application in the evaluation of imbibition mechanisms have not been resolved. In addition, the contact angle sizes on the oil–water wetting walls of the mixed wetting reservoirs also affects the imbibition occurrence and the fluid spatial distribution in tight porous media [26–28]. Yet there is less available information of the imbibition mechanism and oil detachment pattern under the coupling variations of the mixed wetting fraction and the contact angle size scale.

For this investigation, numerical simulation is more suitable. It allows for a systematic parametric analysis of different mixed wetting states and complex boundary conditions, while also ensuring repeatability. The Lattice Boltzmann Method and the direct

Navier–Stokes method are widely used for pore-scale modeling. This is because they provide more reliable predictions of fluid topology and fluid flow [29,30]. Norouzi et al. explore the effect of capillary number (NCap) on the immiscible fluid displacement in porous media by using the Lattice Boltzmann Method (LBM) [31]. Although the LBM can capture fluid flow in three-dimensional irregular porous media, it faces challenges in some cases. For imbibition flow with a low capillary number and a high viscosity ratio, the spurious flow problem at the fluids interface can affect the accuracy of the simulation results [32]. In contrast to LBM, the direct Naiver–Stokes method combined with the phase-field (PF) model, level setting (LS) model, or volume of fluid (VOF) model can accurately track sharp interfaces of high viscosity ratio two-phase fluid flow [33,34]. The phase-field method, with its advantages of more accurate interface tracking, more realistic fluid images, energy conservation in complex pore throats, and lower computational costs, has more extensive application ranges than LS and VOF [35–37]. Even in the low capillary number and high viscosity fluid imbibition flows, numerical results consistent with experimental results can be obtained. Thus, it is essential to employ the phase-field method to perform a detailed investigation of the imbibition mechanisms and regularities for the spatial mixed wetting states to solve the existing uncertainty regarding imbibition potential, oil detachment pattern, as well as critical conditions for different mixed wetting states.

In order to more accurately describe the influence of the various complicated mixed wetting characteristics on the spontaneous imbibition oil recovery effect, capillary models are employed to replace the real porous medium model, which aims to eliminate the influence of complex pore structures. Then this model is validated both numerically with previous simulation results and theoretically by comparing the results with the analytical solutions. Moreover, this work also creatively investigates the influence of the mixed wetting fraction and contact angle size on the imbibition oil recovery regularities, and objectively analyzes the imbibition oil recovery mechanism, fluid flow pattern, and imbibition oil recovery potential for the mixed wetting reservoirs.

2. Methodology

2.1. Mathematical Model Description and Establishment

The pores in rocks are simplified as the horizontal capillary tubes with circular cross-sections of equal diameter. In previous work, a pore-scale mixed wettability model was developed to simulate the imbibition oil recovery process at the pore scale [24]. It was found that the degree of mixed wettability and its distribution have a significant relationship with the imbibition oil recovery rate. During the analysis of residual oil formation, several typical mixed wettability pore channels were identified. To investigate the imbibition behavior in these typical mixed wettability pore throats, the pores in the media are simplified as the horizontal capillary tubes with circular cross-sections of equal diameter. Although the capillary model ignores the complex morphology of real pores, the distribution of pore sizes, connectivity between pores, and irregularities, it can effectively quantify the impact of mixed wettability on the imbibition oil recovery process, thus eliminating the interference introduced by other factors such as the complexity of pore structure. The mineral constituent of a tight oil reservoir is complex and randomly distributed, resulting in the uneven distribution of rock pore surface wettability, which possibly presents different wetting fractions (i.e., water wetting height to diameter ratio, $f_w = h_w/D$) radial along the capillary tube. The mixed wetting capillary tube with a radius of 1 µm and a length of 10 µm is employed as the physical model, as shown in Figure 1. The mixed wetting capillary tube is initially filled with the oil phase. Then the water phase at the left inlet of the capillary tube is continuously imbibed to expel the existing oil phase under the effect of the spontaneous imbibition. The density and viscosity of water are 1 g/cm^3 and 1 mPa·s,

respectively. It is assumed that the density and viscosity of the oil phase are equal to those of the water phase. The interfacial tension of oil–water is 0.035 N/m.
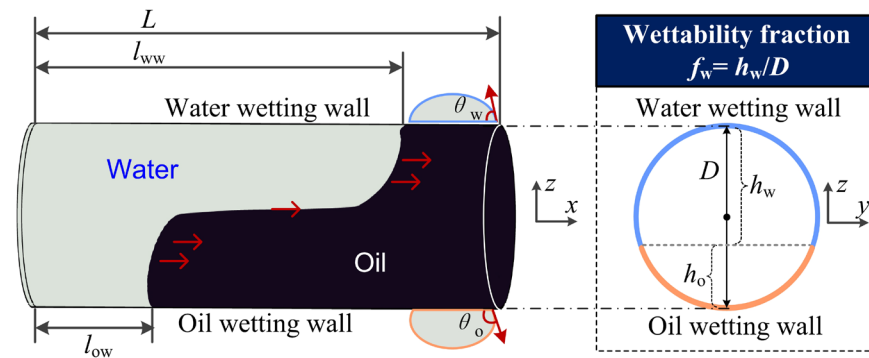
Figure 1. Schematic representation of spatial radial mixed wetting capillary model.

Due to the capillary pressure, water is imbibed into the tiny pore channels of tight oil reservoirs. In the process of spontaneous imbibition, the interfacial effect and dynamic characteristics of two-phase fluid flow in the capillary channel will constantly change. This makes it necessary to take account of the complex moving interface for conserving the mass balance. Based on the phase-field method and interface dynamics mechanism, the Cahn–Hilliard equation together with Navier–Stokes equations is employed to control the spatiotemporal distribution of ordered physical parameters. Without an additional interface reconstruction algorithm, the two-phase moving interface can be obtained by solving the order parameter (ϕ) distribution in the study area [38]. For the imbibition oil recovery simulation, $\phi = -1$ represents that the study region is completely saturated with oil, and the region with $\phi = 1$ is set as water. The Cahn–Hilliard equation can be expressed as two second-order partial differential equations [37]:

$$\frac{\partial \phi}{\partial t} + \mathbf{u} \cdot \nabla \phi = \nabla^2 G \tag{1}$$

$$G = \lambda \left(-\nabla^2 \phi + \frac{(\phi^2 - 1)\phi}{\varepsilon^2} \right) \tag{2}$$

where ϕ is the order parameter. u represents the flow velocity of the fluid. G denotes the chemical potential that is derived from the mixing energy density function [39]. ε represents the thickness of the sharp phase interface. λ represents the mixing energy magnitude. These parameters are related to the surface tension coefficient (σ) through the following equation [36]:

$$\sigma = \frac{2\sqrt{2}\lambda}{3\varepsilon} \tag{3}$$

The convective term in Equation (1) is a non-conservative form that enhances the stability of systems coupled to a momentum equation (fluid flow equation). The non-conservative form is more suitable for investigating the macroscopic-scale flow and generally yields a more easily converged solution. However, when the non-conservative form is applied to the pore-scale two-phase dynamic interface tracking, the accurate numerical conservation of integration of ϕ is difficult to obtain. Obviously, Equation (1) cannot satisfy the current research needs and thus should be converted to a conservative form, which can be expressed as

$$\frac{\partial \phi}{\partial t} + \nabla \cdot (\mathbf{u}\phi) = \nabla^2 G \tag{4}$$

Although the calculation time cost is increased, the conservative form accurately preserves the mass of each fluid and further improves the visual fidelity of the evolution of the fluid phase interface.

The main driving forces of the imbibition in tight rock are the capillary pressure and gravity. However, the effect of gravity on the imbibition can be ignored for the horizontal capillary channels. Therefore, the effect of gravity has not been taken into account in this mathematical model [40]. Assuming that the flow in the spontaneous imbibition process is incompressible, isothermal, and laminar, the Navier–Stokes equation and continuity equation in the micro channel can be given as follows:

$$\rho\frac{\partial \mathbf{u}}{\partial t} + \rho(\mathbf{u}\cdot\nabla)\mathbf{u} = -\nabla p + \mu\nabla^2\mathbf{u} + G\nabla\phi \tag{5}$$

$$\rho\nabla\cdot\mathbf{u} = 0 \tag{6}$$

where p, ρ, and μ are pressure, density, and dynamic viscosity of fluid, respectively.

The volume fractions of fluid 1 and fluid 2 can be calculated by

$$V_{f,2} = \min(\max([(1+\phi)/2], 0), 1)$$
$$V_{f,1} = 1 - V_{f,2} \tag{7}$$

where the min and max operators are used so that the volume fractions have a lower limit of 0 and an upper limit of 1. The physical parameter can be expressed as a linear superposition of two fluids (fluid 1 and 2) by the Heaviside function [41]:

$$\rho = \rho_1 + (\rho_2 - \rho_1)H\left(\frac{V_{f,2}-0.5}{l_\rho}\right)$$
$$\mu = \mu_1 + (\mu_2 - \mu_1)H\left(\frac{V_{f,2}-0.5}{l_\mu}\right) \tag{8}$$

where H is a smooth step function and l is a mixing parameter defining the size of the transition zone.

The solid wall with the wetted wall boundary condition is employed to investigate the two-phase fluid interface movement in the spontaneous imbibition. In addition, it is necessary to ensure that the gradient of chemical potential on the solid wall is zero. Thus, the boundary conditions can be expressed as

$$\mathbf{n}\cdot\varepsilon^2\nabla\phi = \varepsilon^2\cos(\theta_w)|\nabla\phi| \tag{9}$$

$$\mathbf{n}\cdot\gamma G = 0 \tag{10}$$

where $\mathbf{n}$ is the outer normal direction of the wall. θ_w is the contact angle between the fluid and solid wall, reflecting the wettability of the channel wall. γ is the mobility parameter relating to the interface thickness (ε), which can be given as

$$\gamma = \chi\varepsilon^2 \tag{11}$$

where χ is the mobility tuning parameter defined as the velocity-related parameter. The mobility determines the time scale of the Cahn–Hilliard diffusion and must be large enough to retain a constant interfacial thickness but small enough so that the convective terms are not overly damped. For the capillary flow cases, the lower limit of χ of the sharp moving interface can be estimated through the following two equations [42–44]:

$$\chi = \frac{1}{a\sqrt{\mu_e}} = \frac{1}{a\sqrt{\mu_1\mu_2}} \tag{12}$$

$$\chi = \frac{\sqrt{8}\varepsilon}{3\sigma\Delta t} \tag{13}$$

where *a* is a constant, which is usually approximately equal to 10 [39,40]. μ_e is effective viscosity.

Numerical simulation work is implemented by using the COMSOL Multiphysics platform. In this work, the pressure boundaries with a total pressure of 101 kPa are set as the inlet and outlet of the model for the Navier–Stokes equation. The following settings are applied for the boundary conditions in the Cahn–Hilliard equation at the inlet and outlet. At the inlet boundary, a fixed composition (or phase fraction) for the two fluids involved is assumed, allowing for the simulation of a constant flow of the displaced and displacing fluids into the system. This condition ensures that the initial phase distribution at the inlet is well-defined and remains stable throughout the simulation. At the outlet boundary, a zero normal flux condition is applied to the phase field, preventing any phase change or flow of the fluids normal to the outlet boundary. This condition ensures that the phase fraction remains constant at the outlet without affecting the flow dynamics in the simulation domain. These boundary conditions are chosen to accurately reflect the physical nature of the imbibition process, focusing on the impact of wettability and capillary forces. In the calculation process of fluid simulation, the time step size is controlled by a numerical solver, which employs the backward differential formula (BDF). It is noted that the initial time step must be small enough to avoid singularities.

The issue of spurious velocities at the fluid–fluid interface is a well-known challenge in phase-field simulations, particularly when modeling multiphase flows with sharp interfaces. Firstly, the phase-field regularization parameter is chosen to ensure a smooth transition between the two fluids at the interface, which helps avoid sharp gradients that may lead to numerical artifacts, such as spurious currents. By controlling the interface width, unwanted velocity effects are minimized without compromising the accuracy of the phase behavior. Secondly, the mesh is sufficiently refined near the interface to resolve the phase field and fluid properties with high accuracy. This refinement helps capture the fluid–fluid interface more precisely, reducing the likelihood of spurious velocities that often arise from poor resolution at the interface. Additionally, appropriate time-stepping techniques are applied to avoid excessive oscillations in the solution, particularly near the interface, which can generate spurious velocities. Stable time steps are selected, and numerical stabilization methods are employed to ensure the velocity field remains well-behaved throughout the simulation. Finally, the software's built-in interface capturing methods, such as ensuring the continuity of velocity and pressure at the interface, are used to guarantee smooth handling of the fluid–fluid boundary.

2.2. Numerical Model Validation

Simulations with different mesh densities are performed to evaluate the sensitivity of the results to the grid resolution. As shown in Figure 2, the simulation results of oil recovery efficiency at the calculation time of 2.31×10^{-6} s are obtained under different grid resolutions. When the grid cell number is increased to 40,278, the oil recovery efficiency is basically the same. In order to fully ensure grid quality and computational accuracy, and reduce computation time, the mesh generation scheme with this grid cell size is ultimately chosen for subsequent work.
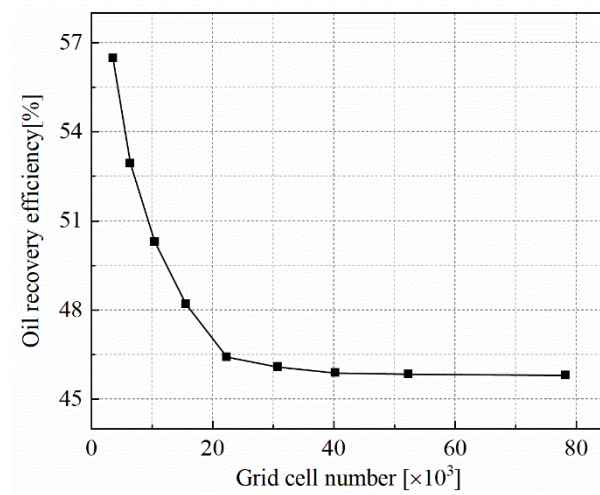
Figure 2. Mesh independence verification.

To validate the reliability and validity of the above-mentioned imbibition model, the capillary imbibition oil recovery process is simulated and compared with the published results [37]. In view of the small pore throat of tight reservoirs, the radius of the two-dimensional long straight capillary is set to 1 μm. The left and right sides of the capillary, as the inlet and outlet of the model, are set at 101 kPa to ensure imbibition. In order to reduce the computational cost, half of the capillary is simulated, so the lower wall of the model is symmetrical. The upper sidewall of the model is the wetted wall, whose contact angle is set to 30° for the model validation in this work. Initially, the entire capillary is saturated with oil. Under the action of capillary pressure, water, as the wetting phase, is imbibed into the capillary to displace the existing oil. The numerical results of a stable meniscus formation and the spontaneous imbibition front widths (i.e., the horizontal distance from the three-phase contact point to the meniscus center point) for different aspect ratios (i.e., the ratio of micro-capillary length to micro-capillary radius) are shown in Figures 3 and 4, which are compared with the corresponding simulation results from Peng [37].
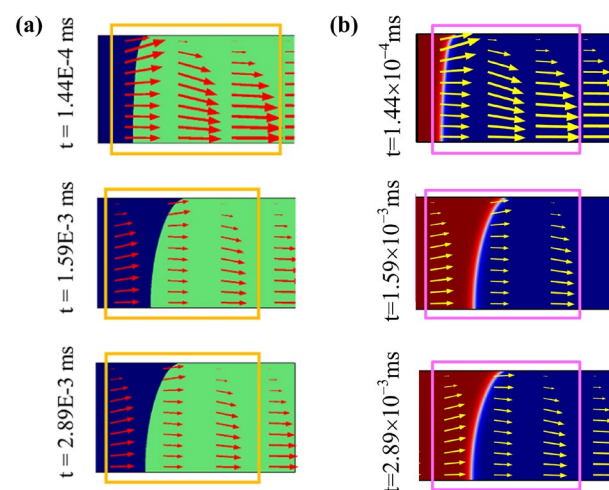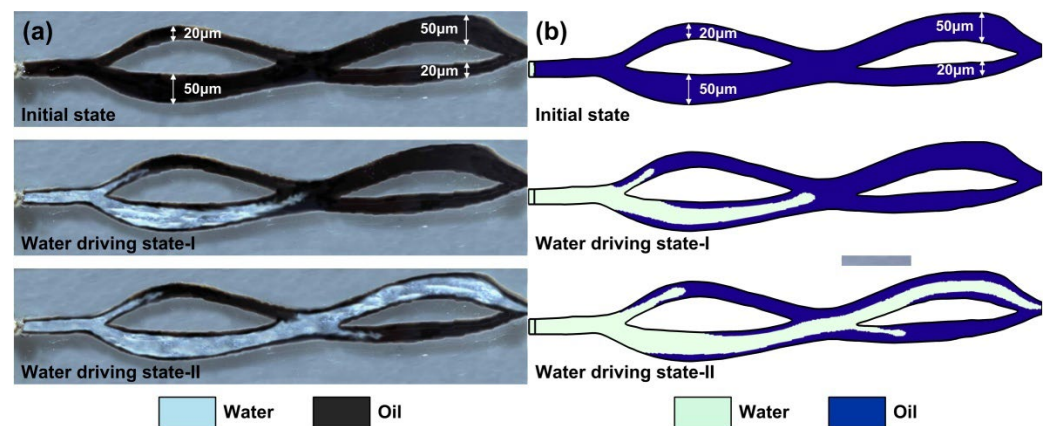

Figure 3. The spontaneous imbibition processes of the micro-capillary with a radius of 1 μm at different time steps when l/R is 5. The arrows denote the velocity magnitudes and directions. (**a**) Results in reference from Peng [37]; (**b**) Numerical results in this work.
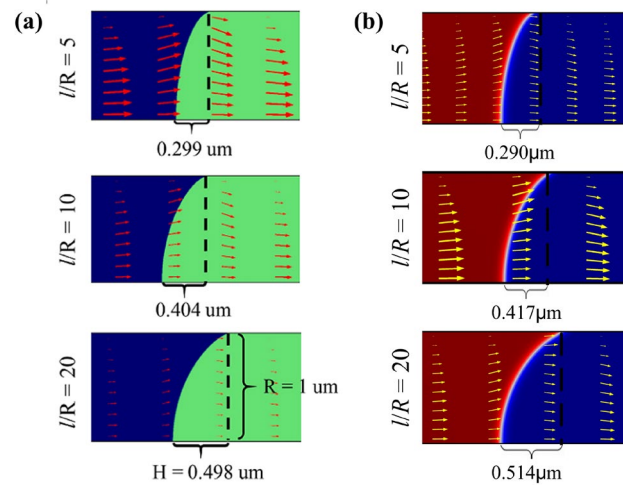
Figure 4. The spontaneous imbibition front widths for different l/R at 2.31×10^{-3} ms. (**a**) Results in reference from Peng [37]; (**b**) Numerical results in this work.

From Figure 3a,b, the formation and stabilization of the oil–water two-phase front meniscus in the spontaneous imbibition process are completely consistent with results from Peng [37]. Meanwhile, the spontaneous imbibition front width values obtained by the proposed model in this paper are 0.290 μm, 0.417 μm, and 0.514 μm, respectively. The results displayed a favorable comparison between the above-mentioned results and published numerical data [37], with an error margin of less than ±3.2% at different aspect ratios.

In order to evaluate the difference between the numerical model prediction results and the actual results in this work, a microfluidic chip design similar to that presented by Sun et al. [45] is created. At the beginning, the entire network of channels in the model is fully saturated with oil. Water is then injected at a controlled flow rate from the left inlet to displace the oil. Figure 5 shows a comparison between the simulation results obtained using the current method and the experimental observations from Sun's study. The results demonstrate that the flow patterns predicted by the simulation closely match the experimental findings, particularly during the middle and later stages of water flooding.


Figure 5. Water/oil displacement processes in microfluidic chip model. (**a**) Experimental result in reference [45]. (**b**) Numerical results in this work.

3. Results and Discussion

3.1. Effect of Wettability Fraction on Spontaneous Imbibition and Oil Production

The effect of the differing spatial distribution of the radial mixed wettability on the spontaneous imbibition patterns and oil production characteristics is investigated. The parameter of wettability fraction f_w is defined in this paper to quantitate the spatial heterogeneity of the radial mixed wetting capillary tubes. Based on the different heights of the water wetting wall along the diameter direction (i.e., z axis), the partitioning schemes are determined, with corresponding f_w values of 1/6, 1/3, 1/2, 2/3, and 5/6, respectively. The resulting oil production characteristics and fluid distributions for different f_w values are portrayed, as shown in Figure 6. For the mixed wetting combination of $\theta_w = 30°$ and $\theta_o = 105°$, the oil in oil wetting and water wetting regions of the capillary tubes is mobilized, as illustrated in Figure 6a. In other words, regardless of the value of f_w, the complete oil detachment modes of spontaneous imbibition are exhibited, ultimately achieving the good spontaneous imbibition effect. It also can be found that the lower f_w is, the smaller the fluid migration velocity in the mixed wetting capillary tube becomes. The reason for this phenomenon is that low f_w results in a high oil wetting wall share, which increases the fluid flow resistance and retards the fluid migration velocity. In addition, the two-phase moving interfaces show the inhomogeneous plastic deformation of the concave and convex meniscus with f_w. Whereas for the cases of the mixed wetting combination with $\theta_w = 30°$ and $\theta_o = 165°$, there is not only a complete oil detachment mode, but also a partial oil detachment mode, as shown in Figure 6b. For the three cases of $f_w = 1/6$, 1/3, and 1/2 of the mixed wetting combination of $\theta_w = 30°$ and $\theta_o = 165°$, the water phase initially invades into the capillary tube and only flows slowly along the water wetting region. Only a small amount of water is sucked in to replace a small quantity of oil around the inlet of the oil wetting region, behaving as the partial oil detachment. For $f_w = 2/3$, there is a significant spontaneous imbibition front distance on the oil wetting wall at 1×10^{-4} s, indicating that a certain amount of oil at the inlet of the oil wetting area is stripped. For $f_w = 5/6$, the oil at both the inlet and outlet of the capillary tube is fully detached, presenting the water saturation filling, and only a small piece of flaky oil is trapped in the bottom oil wetting area in the middle of the capillary tube. These two cases obviously represent the complete oil detachment mode. It is further confirmed that the spontaneous imbibition oil recovery is affected by the wall wettability fraction.

For cases of the radial mixed wetting combinations with $\theta_w = 30°$, $\theta_o = 105°$ and $\theta_w = 30°$, $\theta_o = 165°$, the contribution of oil wetting and water wetting regions to the spontaneous imbibition oil recovery efficiency varies with f_w, as shown in Figure 7. The results indicate that the spontaneous imbibition oil recovery efficiency in the water wetting regions significantly increases with the increase in f_w. Undoubtedly, this is attributed to the increase in the fraction of the water wetting wall. However, the spontaneous imbibition oil recovery efficiency in the oil wetting region first increases and then decreases with f_w. For the weak oil wetting combination (i.e., $\theta_w = 30°$, $\theta_o = 105°$), the maximum contribution of the oil wetting region to spontaneous imbibition oil recovery efficiency can be achieved at $f_w = 1/3$, but can be achieved at $f_w = 2/3$ for the strong oil wetting combination (i.e., $\theta_w = 30°$, $\theta_o = 165°$). This is because at $f_w = 2/3$, a large amount of oil at the inlet of the oil wetting area is stripped off, presenting the complete detachment mode, ultimately achieving the highest contribution to spontaneous imbibition recovery from the oil wetting area.
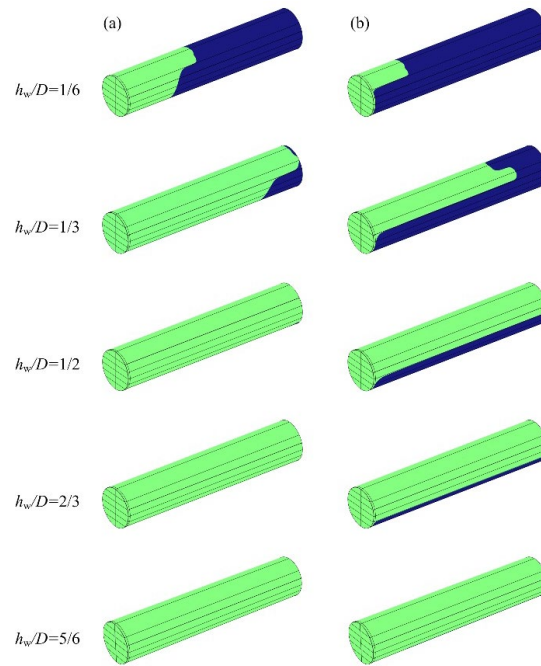
Figure 6. The spontaneous imbibition results of the radial mixed wetting distributions corresponding to different f_w values. Blue and green represent the oil and water, respectively. (**a**) Case for the mixed wetting combination of $\theta_w = 30°$, $\theta_o = 105°$; (**b**) Case for the mixed wetting combination of $\theta_w = 30°$, $\theta_o = 165°$.
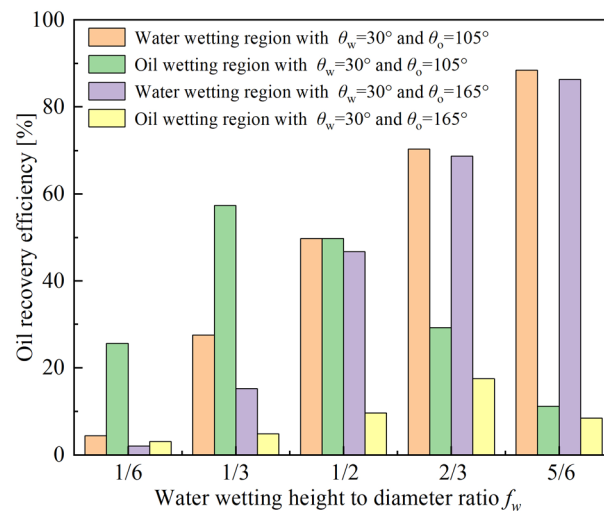

Figure 7. The contribution of the oil wetting and water wetting regions to the spontaneous imbibition oil recovery efficiency at different f_w values for the mixed wetting combination with $\theta_w = 30°$, $\theta_o = 105°$ and $\theta_w = 30°$, $\theta_o = 165°$.

3.2. Effect of Contact Angle on Spontaneous Imbibition and Oil Production

In order to further evaluate the impact of contact angle on the oil detachment mode of spontaneous imbibition, the spatial mixed wetting distribution of $f_w = 1/2$ is selected for the investigation as it eliminates the different wettability proportion influence of oil and the water wetting wall. The contact angle at the water wetting wall ranges from 15° (i.e., strong water wetting) to 75° (i.e., weak water wetting), and is increased 15° per simulation. The contact angle at the oil wetting wall ranges from 105° (i.e., weak oil wetting) to 165° (i.e., strong oil wetting), with an increase step of 15°. The spontaneous imbibition results for different contact angle combinations at 5×10^{-5} s are shown in Figure 8. Based on the observed fluid distribution characteristics during the spontaneous imbibition, there are

basically three typical oil detachment regimes of spontaneous imbibition, mapped on a $\theta_o - \theta_w$ diagram in Figure 8. The approximate boundary marked with the pink dashed line is considered as the boundary between oil complete detachment and partial detachment modes. The approximate boundary marked with the blue dashed line is considered as the boundary between oil partial detachment and trace amount detachment modes. For such a small capillary tube together with a limited number of simulations, it is illogical to specify definite boundaries between different regimes, so the oil imbibition recovery regimes are distinguished by the grayish thick boundary zones to avoid errors caused by the uncertainty. The oil detachment mode, fluid flow regularity, and recovery efficiency of spontaneous imbibition in the three regions are discussed in detail below.
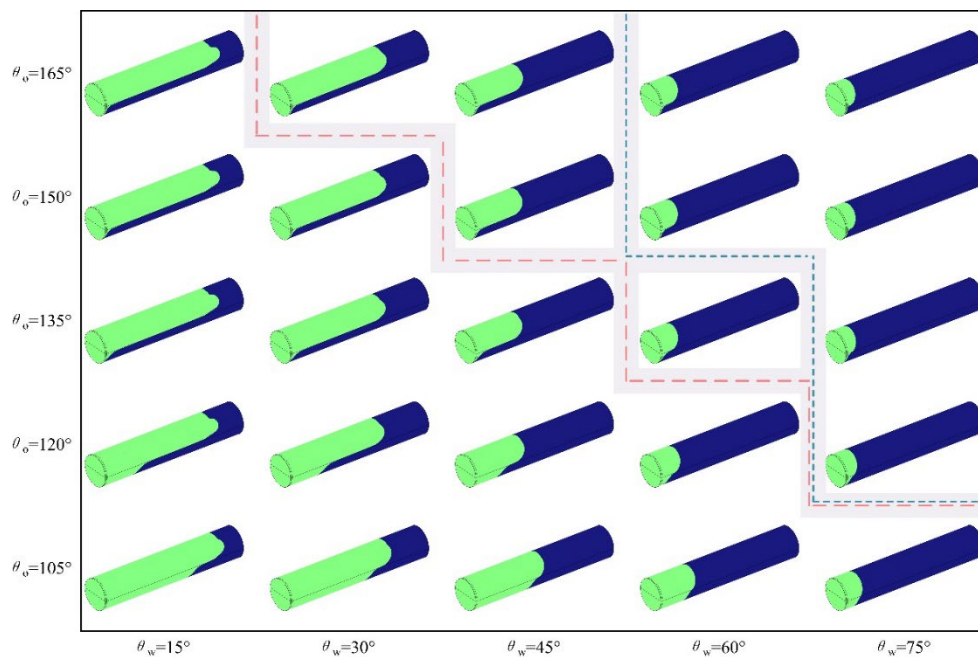

Figure 8. $\theta_w - \theta_o$ diagram showing three oil detachment mode regions of spontaneous imbibition under different wall contact angle size combinations. Green and blue represent the water phase and oil phase, respectively. The boundaries are specified as the thick layers (light gray).

The evolutions of the fluid distribution and variations of the front interfaces for three typical spontaneous imbibition oil detachment modes are shown in Figure 9. For the oil complete detachment cases (as shown in the left lower corner area surrounded by the pink line and block diagram border in Figure 9), the water phase is preferentially filled into the water wetting region of the capillary tube and moves along the water wetting wall in the initial spontaneous imbibition stage. Over time, the oil in the oil wetting part of the capillary tube also begins to gradually be peeled off under the pushing and pulling effect of the upper water phase, but the fluid migration starts a bit later than that in the upper water wetting region, resulting in a significant difference in the two-phase front distance between the water wetting and oil wetting walls in a relative spatial position. Due to this difference, there exists the obvious deformation at the two-phase interface. The imbibition meniscus formed in the mixed wetting capillary tube is a complex combination interface, which is composed of the concave meniscus in the upper and the convex meniscus in the lower part of the capillary tube. After the water breaks through the outlet in the water wetting region of the capillary tube, the oil in the oil wetting region is still constantly stripped until it is completely expelled off. Finally, the capillary tube presents a form of water phase saturated filling, indicating good spontaneous imbibition oil recovery efficiency.
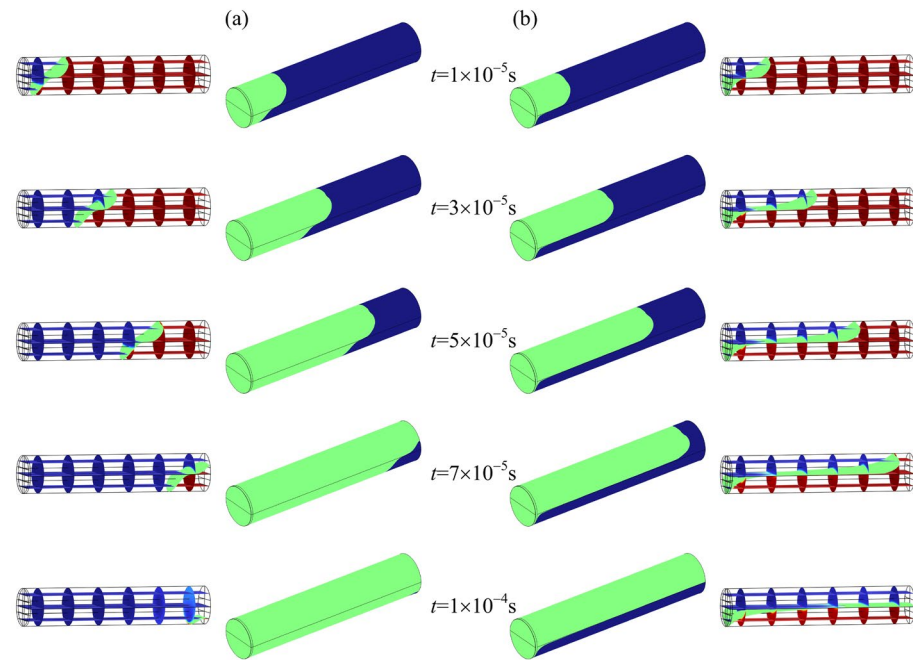
Figure 9. Evolution of the fluid distributions and oil–water interfaces of spontaneous imbibition for the mixed wetting capillary tube at different times. (**a**) Case for the mixed wetting combination of $\theta_w = 30°$, $\theta_o = 105°$; (**b**) Case for the mixed wetting combination of $\theta_w = 30°$, $\theta_o = 165°$.

In order to further observe the dynamic changes in the spontaneous imbibition front interface in the oil complete detachment mode, the migration distance curves of the water phase front on the water wetting wall and the oil wetting wall located in the relative positions (i.e., lines AB and MN) are portrayed in Figure 10. The results indicate that the spacing between these two curves increases over time at the beginning of spontaneous imbibition. After that, the spacing between these two curves remains constant with increasing time, behaving approximately parallel until breakthrough at the outlet. Whereas the approximate constant of the spacing between these two curves is considered to be the front distance difference (ΔL), the magnitude of which is dependent on the contact angle of the mixed wetting capillary tube wall.
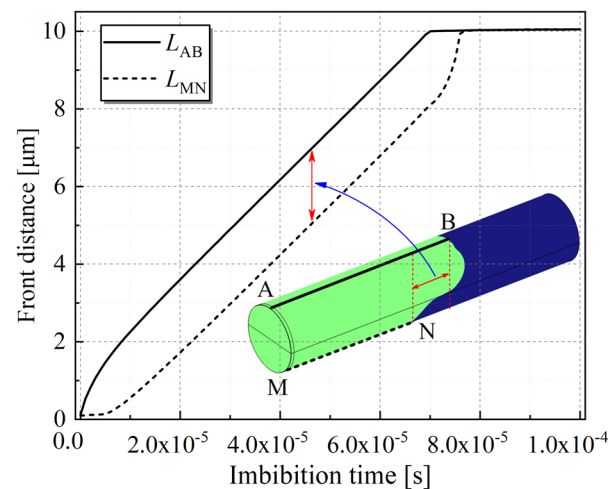
Figure 10. The front migration distances on the water wetting wall and the oil wetting wall located in the relative positions (i.e., lines AB and MN) for the mixed wetting capillary tube with the combination of $\theta_w = 30°$ and $\theta_o = 05°$.

This can be confirmed in Figure 11, where the stable front distance difference values varying with the contact angle sizes are shown. The reason for selecting the value of $\theta_o = 105°$ is that at this point, the oil in spontaneous imbibition cases with arbitrary θ_w values have completely started up and front distances on the two wetting walls of the mixed wetting capillary tube change significantly over time. Furthermore, we observe that a higher water wetting contact angle leads to a reduction in the front distance difference, which is consistent with theoretical expectations. This reduction occurs because, in cases with weaker water wetting, the capillary force driving the imbibition process is weaker, resulting in a lower migration velocity of the front. This slower movement of the front translates to a significantly longer breakthrough time for the water phase in weak water wetting systems compared to those with stronger water wetting behavior. In contrast, in systems with stronger interaction between oil and water, the spontaneous imbibition process enhances oil recovery efficiency, especially at breakthrough. The analysis indicates that as the contact angle of the water wetting wall increases from 15° to 75°, the oil recovery efficiency via spontaneous imbibition improves by 9.52%. This suggests that a more pronounced water wetting behavior accelerates the displacement of oil, facilitating the recovery process. Additionally, the effect of prolonged spontaneous imbibition time on the remaining oil in the corners of the capillary tube is noteworthy. As imbibition time increases, the remaining oil, which is trapped in the capillary corners, is gradually displaced and stripped by the advancing water phase. This phenomenon significantly contributes to the ultimate oil recovery efficiency, as the process continues to enhance the displacement of residual oil, leading to further improvements in spontaneous imbibition oil recovery. In summary, the fluid velocity and interface behavior during spontaneous imbibition are strongly influenced by the contact angle of the wetting walls, and an increase in the water wetting contact angle leads to more efficient oil recovery. The dynamic changes in the front distance and the interaction between oil and water further highlight the importance of optimizing the contact angle to enhance imbibition efficiency and overall oil recovery performance.
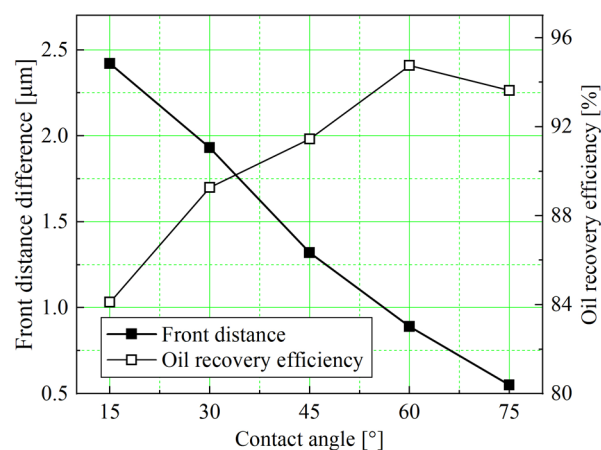
Figure 11. The stable front distance difference as a function of the contact angle for the mixed wetting capillary tubes with $\theta_o = 105°$.

To further quantify the effect of different oil detachment modes of spontaneous imbibition, the oil recovery efficiencies in the two wetting regions of mixed wetting capillary tubes are compared, as shown in Figure 12. It can be observed that at arbitrary θ_w, the contribution of the water wetting region to spontaneous imbibition recovery efficiency is significantly greater than that of the oil wetting region. In addition, at a particular θ_o of 165°, the spontaneous imbibition oil recovery factor for both regions decreases as θ_w increases. Obviously, in the strong water wetting cases (i.e., the values of θ_w are 15°, 30°, and 45°),

the water wetting region achieves a good spontaneous imbibition effect and also drives the peel-off of the partial oil in the oil wetting region, which corresponds to the wetting characteristics of the top left area enclosed by the blue line in Figure 8. However, when in weak water wetting states (i.e., the values of θ_w are 60° and 75°), the overall spontaneous imbibition oil recovery efficiency in both the water wetting and oil wetting regions is less than 10%, ultimately exhibiting poor spontaneous imbibition effects, which corresponds to the wetting characteristics of the top right area enclosed by the blue line in Figure 8. These phenomena can be attributed to the influence of the wall contact angle size scale.
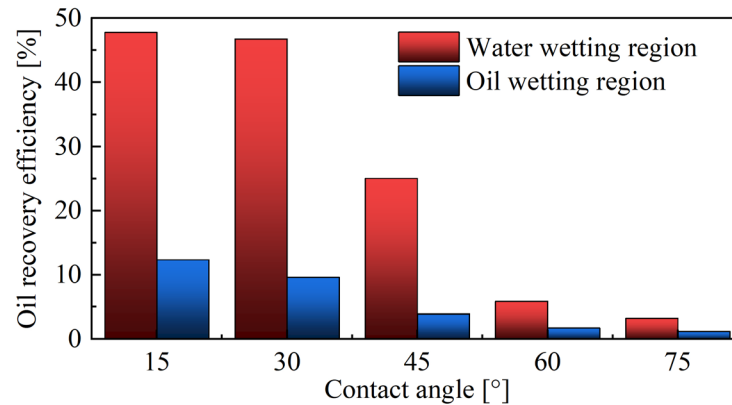
Figure 12. The histogram of quantitative spontaneous imbibition oil recovery efficiency for oil wetting region and water wetting region for the mixed wetting capillary tube with $\theta_o = 165°$.

3.3. Effect of Oil Viscosity on Spontaneous Imbibition Front Distance Difference

The effect of the oil viscosity on the spontaneous imbibition front distances on the two relative wetting sidewalls of the mixed wetting capillaries are investigated, as shown in Figure 13. The oil viscosity varies from 1 mPa·s to 20 mPa·s. The contact angles on the water wetting and oil wetting sidewalls of the capillaries are 30° and 105°, respectively. Moreover, the water wetting ratio is 1/2, meaning that the mixed wetting capillary is symmetric. Due to the non-uniform wetting characteristic of the mixed wetting capillary, there still exists asymmetric filling behavior and different fluid front distances on two wetting sidewalls for a series of different viscosity ratio cases. And the greater oil viscosity enhances the front distance difference, but little viscosity difference reduces this behavior.
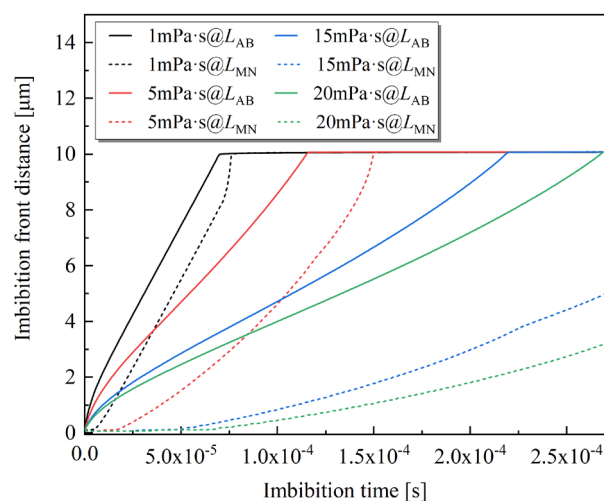
Figure 13. The effect of oil viscosity on the spontaneous imbibition front distances on the two relative wetting sidewalls of the mixed wetting capillaries.

4. Conclusions

In this work, we investigate the oil detachment modes and recovery efficiency of spontaneous imbibition in the mixed wetting capillary channels. This research emphasizes the comprehensive influence of the wettability fraction and contact angle size scale on spontaneous imbibition oil recovery. By analyzing the capillary spontaneous imbibition effects of five mixed wetting distribution modes corresponding to different f_w values, we show that there are oil complete detachment and partial detachment modes of spontaneous imbibition. These oil detachment modes are determined by the combined effects of mixed wetting fractions and wall contact angle sizes. For the mixed wetting capillary with strong oil wetting, when f_w is low, this leads to the partial detachment mode of spontaneous imbibition oil recovery.

We further investigate the influence of different contact angle sizes on the spontaneous imbibition effects of the mixed wetting capillary tubes. A $\theta_w - \theta_o$ diagram for determining the spontaneous imbibition oil detachment modes in the symmetrical mixed wetting systems (namely $f_w = 1/2$) is built up. It generally classifies three typical imbibition oil recovery modes, including oil complete detachment, partial detachment, and local disturbance. For the oil complete detachment mode, the capillary tube exhibits a water phase saturated filling, achieving the optimal spontaneous imbibition effect. The oil partial detachment modes have relatively poor spontaneous imbibition oil recovery effects due to a certain amount of the continuous flake-shaped oil being trapped. It should be noted that for mixed wetting capillary tubes with a combination of weak water wetting and strong oil wetting, local spontaneous imbibition turbulence can only detach very little oil at the inlet of the water wetting area, ultimately achieving a recovery efficiency of less than 10%. Moreover, it also can be observed that the different wall wettabilities of the mixed wetting capillary tube result in the different front distances on two wetting walls. Obviously, there is a significant front distance difference for the mixed wetting capillary tube, the size of which is influenced by the coupling effect of two different contact angles on the capillary walls. Although this work primarily focuses on imbibition oil recovery in mixed wetting capillary channels, the principles and results can be applied to pore network models. In our previous work, a numerical model for spontaneous imbibition at the pore scale was established, and the imbibition and oil recovery process at the pore scale was simulated. The relationship between the degree and distribution of mixed wettability and the oil recovery rate through imbibition has been elucidated, along with the imbibition behavior in typical mixed wetting pore throat channels.

Author Contributions: Conceptualization, E.Y.; methodology, Y.P.; software, Y.P.; validation, D.W.; formal analysis, D.W.; investigation, Y.P.; resources, E.Y.; data curation, D.W.; writing—original draft preparation, Y.P.; writing—review and editing, D.W.; visualization, Y.P.; supervision, E.Y.; project administration, D.W.; funding acquisition, E.Y. and Y.P. All authors have read and agreed to the published version of the manuscript.

Data Availability Statement: The data presented in this study are available on request from the corresponding author (the data are not publicly available due to resource intensive).

Conflicts of Interest: The authors declare that they have no conflicts of interest.

References

1. Wei, B.; He, X.; Li, X.; Ju, Y.; Jin, J.; Luo, Q. Residual oil contents of dolomicrite and sandy dolomite tight oil reservoirs after CO_2 huff and puff: An experimental study. *Energy* **2023**, *275*, 127510. [CrossRef]
2. Hu, S.; Tao, S.; Wang, M.; Pang, Z.; Bai, B.; Chen, Y.; Lu, S.; Chen, Y.; Yang, Y.; Jin, X.; et al. Migration and accumulation mechanisms and main controlling factors of tight oil enrichment in a continental lake basin. *Petrol. Explor. Dev.* **2023**, *50*, 547–557. [CrossRef]
3. Peng, X.; Wang, X.; Zhou, X.; Lin, Z.; Zeng, F.; Huang, X. Lab-on-a-chip systems in imbibition processes: A review and applications/issues for studying tight formations. *Fuel* **2021**, *306*, 121603. [CrossRef]
4. Song, Z.; Song, Y.; Li, Y.; Bai, B.; Song, K.; Hou, J. A critical review of CO_2 enhanced oil recovery in tight oil reservoirs of North America and China. *Fuel* **2020**, *276*, 118006. [CrossRef]
5. Meng, Q.; Liu, H.; Wang, J. A critical review on fundamental mechanisms of spontaneous imbibition and the impact of boundary condition, fluid viscosity and wettability. *Adv. Geo-Energy Res.* **2017**, *1*, 1–17. [CrossRef]
6. Wang, X.; Peng, X.; Zhang, S.; Du, Z.; Zeng, F. Characteristics of oil distributions in forced and spontaneous imbibition of tight oil reservoir. *Fuel* **2018**, *224*, 280–288. [CrossRef]
7. Ghosh, T.; Sekhar, G.P.R.; Deb, D. Mathematical modeling of co-current spontaneous imbibition in heterogeneous porous medium. *Eur. J. Mech. B Fluid* **2019**, *76*, 81–97. [CrossRef]
8. Siebold, A.; Nardin, M.; Schultz, J.; Walliser, A.; Oppliger, M. Effect of dynamic contact angle on capillary rise phenomena. *Colloid. Surface A* **2000**, *161*, 81–87. [CrossRef]
9. Zhong, J.; Duan, H.; Wang, J.; Ma, B.; Sun, Z.; Yao, J. Simulation of water self-imbibition in na-nometer throat-pore structure filled with oil. *Geo. Sci. Eng.* **2023**, *221*, 211370.
10. Zhang, T.; Li, Z.; Gao, M.; Wang, L.; Adenutsi, C.D.; You, O. Experimental and numerical simulation research on counter-current imbibition distance in tight oil reservoirs. *J. Mol. Liq.* **2023**, *389*, 122791. [CrossRef]
11. Sukee, A.; Nunta, T.; Haruna, M.A.; Kalantariasl, A.; Tangparitkul, S. Influence of sequential changes in the crude oil-water interfacial tension on spontaneous imbibition in oil-wet sandstone. *J. Petrol. Sci. Eng.* **2022**, *210*, 110032. [CrossRef]
12. Xu, D.; Bai, B.; Wu, H.; Hou, J.; Meng, Z.; Sun, R.; Li, Z.; Kang, W. Mechanisms of imbibition enhanced oil recovery in low permeability reservoirs: Effect of IFT reduction and wettability alteration. *Fuel* **2019**, *244*, 110–119. [CrossRef]
13. Artem, B.; Ben, C.; Rossen, S.; Iko, B.; John, R.; Mark, R.; David, D.; Keyu, L. Experimental investigations of the wettability of clays and shales. *J. Geophys. Res Sol. EA* **2009**, *114*, B07202.
14. Dekker, L.W.; Ritsema, C.J. How water moves in a water repellent sandy soil: 1. potential and actual water repellency. *Water Resour. Res.* **1994**, *30*, 2507–2517. [CrossRef]
15. Yassin, M.R.; Dehghanpour, H.; Wood, J.; Lan, Q. A theory for relative permeability of unconventional rocks with dual-wettability pore network. *SPE J.* **2016**, *21*, 1970–1980. [CrossRef]
16. Yassin, M.R.; Begum, M.; Dehghanpour, H. Organic shale wettability and its relationship to other petrophysical properties: A Duvernay case study. *Int. J. Coal Geol.* **2017**, *169*, 74–91. [CrossRef]
17. Shi, Y.; Yassin, M.R.; Yuan, L.; Dehghanpour, H. Modelling imbibition data for determining size distribution of organic and inorganic pores in unconventional rocks. *Int. J. Coal Geol.* **2019**, *201*, 26–43. [CrossRef]
18. Shi, H.; Luo, X.; Li, X.; Liu, N.; Qi, Y.; Fang, T.; Zhang, L.; Lei, Y. Effects of mix-wet porous me-diums on gas flowing and one mechanism for gas migration. *J. Petrol. Sci. Eng.* **2017**, *152*, 60–66.
19. Wang, J.; Liu, H.; Qian, G.; Peng, Y.; Gao, Y. Investigations on spontaneous imbibition and the influ-encing factors in tight oil reservoirs. *Fuel* **2019**, *236*, 755–768.
20. Cai, J.; Chen, Y.; Liu, Y.; Li, S.; Sun, C. Capillary imbibition and flow of wetting liquid in irregular capillaries: A 100-year review. *Adv. Colloid Interfac.* **2022**, *304*, 102654. [CrossRef]
21. Kurotoria, T.; Murugesu, M.P.; Zahasky, C.; Vega, B.; Druhan, J.L.; Benson, S.M.; Kovscek, A.R. Mixed imbibition controls the advance of wetting fluid in multiscale geological media. *Adv. Water. Resour.* **2023**, *175*, 104429. [CrossRef]
22. Bartels, W.B.; Rucker, M.; Boone, M.; Bultreys, T.; Mahani, H.; Berg, S.; Hassanizadeh, S.M.; Cnudde, V. Imaging spontaneous imbibition in full Darcy-scale samples at pore-scale resolution by fast X-ray tomography. *Water Resour. Res.* **2019**, *55*, 7072–7085. [CrossRef]
23. Jiang, Z.; Li, G.; Zhao, P.; Zhou, Y.; Mao, Z.; Liu, Z. Study on spontaneous imbibition and dis-placement characteristics of mixed-wet tight sandstone reservoir based on high-precision balance and NMR method. *Fuel* **2023**, *345*, 128247. [CrossRef]
24. Pu, Y.; Yang, E.; Du, Q. Effect of mixed wettability of tight reservoirs on the pore scale imbibition law. *J. Northe. Petrol. Univ.* **2024**, *48*, 86–95.
25. Xiao, Y.; Zheng, J.; He, Y.; Wang, L. Percolation transitions of spontaneous imbibition in fractional-wet porous media. *Colloid. Surface A* **2023**, *673*, 131826. [CrossRef]
26. Wang, L.; Ma, F.; He, Y.; Liu, D. The prediction of spontaneous oil-water imbibition in composite capillary. *Petroleum* **2022**, *8*, 84–91. [CrossRef]

27. Wang, L.; He, Y.; Xiao, Y.; Wang, H.; Ma, F. Spontaneous Gas-Water Imbibition in Mixed-Wet Pores. *Petrophysics* **2020**, *61*, 230–238. [CrossRef]

28. Qi, Y.; Luo, X.; He, Y.; Dang, H.; Liu, N.; Lei, Y.; Zhang, L. Experimental studies on oil imbibition in mixed-wetting porous medium. *Chin. J. Geol.* **2015**, *50*, 1208–1217.

29. Alpak, F.O.; Berg, S.; Zacharoudiou, I. Prediction of fluid topology and relative permeability in imbibition in sandstone rock by direct numerical simulation. *Adv. Water. Resour.* **2018**, *122*, 49–59. [CrossRef]

30. Soleimani, R.; Norouzi, S.; Rasaei, M.R. Investigation of gas condensate drop-out effect on gas relative permeability by Lattice Boltzmann modelling. *Can. J. Chem. Eng.* **2019**, *97*, 1921–1930. [CrossRef]

31. Norouzi, S.; Soleimani, R.; Farahani, M.V.; Rasaei, M.R. Pore-Scale Simulation of Capillary Force Effect in Water-Oil Immiscible Displacement Process in Porous Media. In *81st EAGE Conference and Exhibition*; EAGE Publishing BV: London, UK, 2019; pp. 1–5.

32. Zhao, B.; MacMinn, C.W.; Primkulov, B.K.; Chen, Y.; Valocchi, A.J.; Zhao, J.; Kang, Q.; Bruning, K.; McClure, J.E.; Miller, C.T.; et al. Comprehensive comparison of pore-scale models for multiphase flow in porous media. *Proc. Natl. Acad. Sci. USA* **2019**, *116*, 13799–13806. [CrossRef] [PubMed]

33. Budaraju, A.; Phirani, J.; Kondaraju, S.; Bahga, S.S. Capillary Displacement of Viscous Liquids in Geometries with Axial Variations. *Langmuir* **2016**, *32*, 10513–10521. [CrossRef] [PubMed]

34. Movahedi, H.; Farahani, M.V.; Masihi, M. Development of a Numerical Model for Single- and Two-Phase Flow Simulation in Perforated Porous Media. *J. Energ. Resour. ASME* **2020**, *142*, 042901. [CrossRef]

35. Zhu, G.; Yao, J.; Zhang, L.; Sun, H.; Li, A.; Shams, B. Investigation of the Dynamic Contact Angle Using a Direct Numerical Simulation Method. *Langmuir* **2016**, *32*, 11736–11744. [CrossRef]

36. Yue, P.; Feng, J.; Liu, C.; Shen, J. A diffuse-interface method for simulating two-phase flows of complex fluids. *J. Fluid. Mech.* **2004**, *515*, 293–317. [CrossRef]

37. Peng, X.; Wang, X.; Du, Z.; Zeng, F. Phase-field simulations of precursor film in microcapillary imbibition for liquid-liquid systems. *Int. J. Multiphas. Flow* **2021**, *144*, 103789. [CrossRef]

38. Sun, Y.; Bao, C.; Jiang, Z.; Zhang, X.; Gao, T. A two dimensional numerical study of liquid water breakthrough in gas diffusion layer based on phase field method. *J. Power Sources* **2020**, *448*, 227352. [CrossRef]

39. Cahn, J.W.; Hilliard, J.E. Free energy of a nonuniform system. II. Thermodynamic basis. *J. Chem. Phys.* **1958**, *28*, 258–267. [CrossRef]

40. Zhang, S.; Pu, H.; Zhao, J.X. Experimental and numerical studies of spontaneous imbibition with different boundary conditions: Case studies of middle Bakken and Berea cores. *Energy Fuels* **2019**, *33*, 5135–5146. [CrossRef]

41. Grave, M.; Coutinho, A.L.G.A. Comparing the convected level-set and the Allen Cahn phase-field methods in AMR/C simulations of two phase flows. *Comput. Fluids* **2022**, *244*, 105569. [CrossRef]

42. Kusumaatmaja, H.; Hemingway, E.J.; Fielding, S.M. Moving contact line dynamics: From diffuse to sharp interfaces. *J. Fluid Mech.* **2015**, *788*, 209–227. [CrossRef]

43. Omori, T.; Kajishima, T. Apparent and microscopic dynamic contact angles in confined flows. *Phys. Fluids* **2017**, *29*, 112107. [CrossRef]

44. Yue, P.; Zhou, C.; Feng, J.J.; Ollivier-Gooch, C.F.; Hu, H.H. Phase-field simulations of interfacial dynamics in viscoelastic fluids using finite elements with adaptive meshing. *J. Comput. Phys.* **2006**, *219*, 47–67. [CrossRef]

45. Sun, Z.; Wu, X.; Kang, X.; Lu, X.; Li, Q.; Jiang, W.; Zhang, J. Comparison of oil displacement mechanisms and performances between continuous and dispersed phase flooding agents. *Petrol. Explor. Dev.* **2019**, *46*, 121–129. [CrossRef]